NSRRC - J05258 (2016)

ACES Asian Chemical Editorial Society

DOI: 10.1002/asia.201600543

CHEMISTRY
AN ASIAN JOURNAL
Communication

Fullerene

Conformational Preferences and the Phase Stability of Fullerene Hexa-adducts

San-Lien Wu[+],[a] Chen-Yang Hong[+],[a] Kuan-Yi Wu,[a] Shih-Ting Lan,[a] Chou-Ting Hsieh,[a] Hsin-Lung Chen,[b] and Chien-Lung Wang*[a]

Abstract: Molecular conformation and the assembly structure determine the spatial arrangements of the constituent units and the functions of a molecule. Although, fullerene hexa-adducts (FHAs) have been known as functional materials with great versatility, their conformational preferences and phase stability remain a complicate issue. By choosing bithiophene (T_2) and dodecyl bithiophene ($C_{12}T_2$) as the peripheral units of FHA, and using microscopic, scattering and diffraction characterizations, our study reveals how the intramolecular interaction and environmental stimulus affects the conformational preferences and phase stability of FHAs.

The conformational preference of a molecule determines its three-dimensional (3D) physical structure and whether or not proper molecular functions can be expressed. For instance, biological functions are delivered by biomolecules in specific conformations, such as helixes, sheets, hairpins, and so forth. The functions of artificial molecules also depend on their conformations.[1] Factors, including molecular architectures,[2] degree of polymerization,[1a] solvent properties,[1b] concentration of coordinated ions,[1c] and electrostatic force,[3] have been applied in different molecular systems to exert control over the hierarchical physical structures across multiple length scales.

The development of fullerene chemistry facilitates the functionalization of [60-I_h]-fullerene (C_{60}),[4] and made the functionalized C_{60} derivatives an important building block of many novel molecular systems.[4b,5] Functional materials like amphiphilic fullerene hexa-adducts (FHAs),[5e,f] photoactive FHAs,[5b,6] electroactive FHAs,[7] bioactive FHAs,[8] giant surfactants,[9] and semiconducting giant molecules[10] have been synthesized, and unique supramolecular assembles, including helical supramolecular columns,[5a] supramolecular double cables,[10] smectic A phase,[5c,d] chiral nematic phase,[5g,i] micelles, and vesicles,[5h,9] were observed among these molecules. The conformation of the C_{60}-based molecules is essential to its self-organization behaviors and its material properties because conformational changes can affect the distances among the peripheral functional groups and molecular shapes. However, the conformational preferences and conformer stabilities of the FHAs remain an unclear issue, because the huge size,[5a] and strong physical interactions[3,5c,g] of the peripheral groups of FHAs often dominate the phase formation and obscure the behaviors of the FHA core. To reveal the conformational preferences of the FHAs, in this work, we chose bithiophene as the peripheral functional groups, because of its moderate assembly tendency. Compared to 4-phenylbenzonitrile, which has a melting temperature (T_m) of 87 °C,[5c] the T_m of T_2 is at 32 °C, suggesting a weaker intermolecular interaction. By comparing the phase behaviors of two FHAs, **$C_{12}T_2$-FHA** and **T_2-FHA** in Figure 1a, we are able to show the conformational preferences of the FHAs and the relative stability of their conformers in this work.

The two FHAs are constructed with a spherical C_{60} core and 12 peripheral arms. The peripheral arm, T_2, is made of a propoxycarbonyl linker and a 1-([2,2′-bithiophen]-5-yl)-1H-1,2,3-triazole unit; and the other peripheral arm, $C_{12}T_2$, is made of the same linker and the 4-(5′-dodecyl-[2,2′-bithiophen]-5-yl)-1H-1,2,3-triazol-1-yl unit. Because the propoxycarbonyl linker is

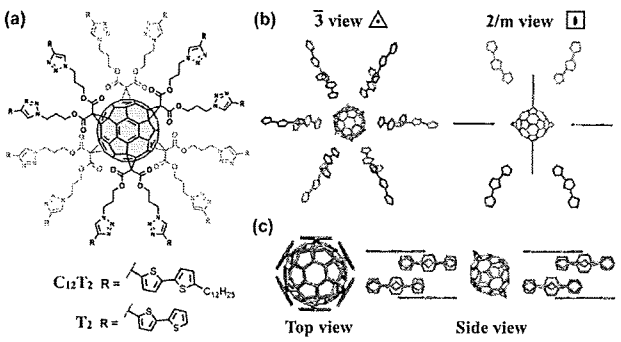

Figure 1. (a) Chemical structure of **$C_{12}T_2$-FHA** and **T_2-FHA**. Illustrations of (b) the star conformation and (c) the rod conformation. In the $\bar{3}$ view, the six blue T_2 groups point upward, and the other six brown T_2 groups point downward.

[a] S.-L. Wu,[+] C.-Y. Hong,[+] K.-Y. Wu, S.-T. Lan, C.-T. Hsieh, Prof. C.-L. Wang
Department of Applied Chemistry
National Chiao Tung University
1001 Ta Hsueh Rd., Hsinchu 30010 (Taiwan)
E-mail: kclwang@nctu.edu.tw

[b] Prof. H.-L. Chen
Department of Chemical Engineering and Frontier Research Center on Fundamental and Applied Sciences of Matters, National Tsing Hua University, Hsin-Chu 30013 (Taiwan)

[+] These authors contributed equally to this work.

Supporting information for this article can be found under http://dx.doi.org/10.1002/asia.201600543.

© 2016 Wiley-VCH Verlag GmbH & Co. KGaA, Weinheim

flexible, the conformational isomerization of the linkers changes the relative positions and orientations of the peripheral arms. Depending on the conformations taken by the 12 peripheral arms, a FHA can have two symmetrical conformations, the star and rod conformation (Figure 1b–1c), and numerous distorted spherical conformations in-between. The star conformation has the T_h symmetry. Viewing $\bar{3}$ and 2/*m* axes (Figure 1b), it can be found that the 12 T_2 arms are spread uniformly in the 3D space. Because the inter-arm distance is maximized in the star conformation, the intramolecular interaction among the peripheral arms is expected to be minimized. Contracting the 6 peripheral arms of a FHA to the top of the C_{60} core, and the other 6 arms to the bottom, turns the T_h star conformation into a C_3 rod conformation (Figure 1c). The rod conformation provides shorter inter-arm distances and stronger intramolecular interactions. Considering the different degrees of physical interaction among the peripheral arms, the conformers of the FHAs (star, rod, and distorted spheres) may have different degrees of thermodynamic stability and will be discussed below.

$C_{12}T_2$-FHA and **T_2-FHA** were synthesized according to Scheme 1. The products have been fully characterized by ^{1}H NMR, ^{13}C NMR, and MALDI-TOF mass spectrometry. To obtain sufficient amount of the stable prefunctionalized FHA, hexa(bis((3-bromopropoxy)carbonyl)methano)fullerene (**Br-FHA**) was synthesized by reacting C_{60} with bis(3-bromopropyl)-malonate through Bingel reaction.[11] The **Br-FHA** was then reacted with NaN_3 in *N,N*-dimethylformamide (DMF) to give hexa(bis((3-azidopropoxy)carbonyl)methano)fullerene (**N_3-FHA**) in 97% yield. The up-field shift of the H_b, H_c in the ^{1}H NMR spectrum (Figure S3 in the SI) indicates that the Br groups have been substituted by the N_3 groups.[12] The obtained **N_3-FHA** was immediately used to react with 5-trimethylsilylethynyl-5′-n-dodecyl-2,2′-bithiophene (**1a**),[13] and ([2,2′-bithiophen]-5-ylethynyl)trimethylsilane (**1b**),[14] through a copper-catalyzed azide–alkyne cycloaddition (CuAAC) to afford the formation of the final products.[15] In the ^{1}H NMR spectra of **$C_{12}T_2$-FHA** and **T_2-FHA** (Figure S4(a), S5(a) in the SI), the integration ratio for the protons on the linker unit, triazole unit, and bithiophene unit (H_b:H_d:H_e in Figure S4(a), S5(a) in the SI) was found to be 2:1:1, respectively, indicating that all the N_3 groups of **N_3-FHA** have been converted into the $C_{12}T_2$, or the T_2 arms. Moreover, in the ^{13}C NMR spectra (Figure S4(b), S5(b) in the SI), the two ^{13}C signals at around $\delta = 141$ and 145 ppm are the characteristic peaks, which belong to the sp^2 carbons on the C_{60} core of a T_h-symmetrical FHA,[16] and the FTIR spectra in Figure S6 show the disappearance of the azide absorption (at $\approx 2100\ cm^{-1}$). The *m/z* values of the products measured from the MALDI-TOF MS spectra in Figure S7 also match the theoretical ones. These results thus confirm the successful formation of the final products.

To investigate the conformation and solid-state phases of the FHAs, thin films of **$C_{12}T_2$-FHA** and **T_2-FHA** were studied by optical microscope (OM) and transmission electron microscope (TEM). As shown in Figure S8, a honeycomb (HC) array was observed in the drop-casted film prepared from the carbon disulfide (CS_2) solution (1 mg mL^{-1}) of **$C_{12}T_2$-FHA**. Under polarized optical microscope (POM), the HC array is completely dark, indicating that the **$C_{12}T_2$** arms of the **$C_{12}T_2$-FHA** molecules are randomly oriented in the film. Highly ordered HC array can be prepared from the CS_2 solution (1 mg mL^{-1}) of **$C_{12}T_2$-FHA**. The scanning electron microscope (SEM) image in Figure 2a con-

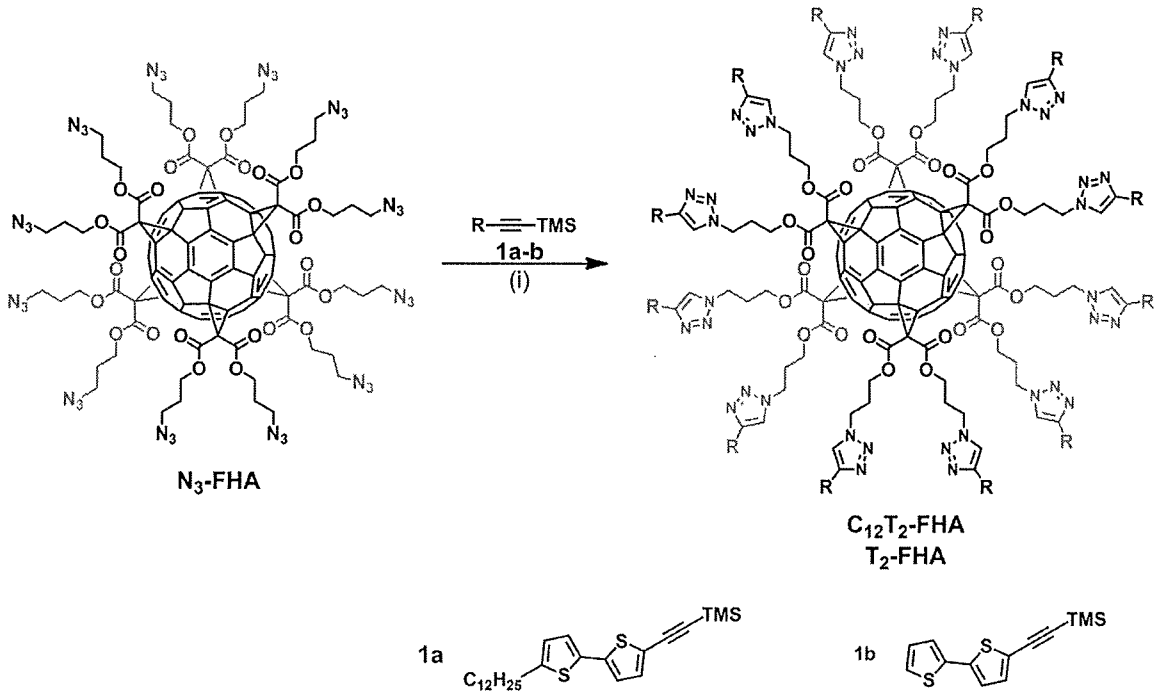

Scheme 1. Synthetic route of the FHAs. (i) TBAF, $CuSO_4{\cdot}5H_2O$, sodium ascorbate, CH_2Cl_2, H_2O, 12 h. (Yield: **$C_{12}T_2$-FHA**: 59%, **T_2-FHA**: 59%).

© 2016 Wiley-VCH Verlag GmbH & Co. KGaA, Weinheim

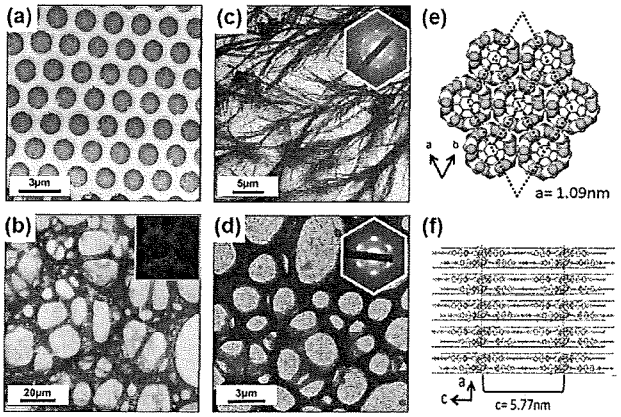

Figure 2. (a) SEM image of the HC array of $C_{12}T_2$-FHA. (b) The OM and POM images of T_2-FHA drop-casted film. TEM images and ED patterns of (c) $C_{12}T_2$-FHA and (d) T_2-FHA crystal. (e) [001] and (f) [010] views of the trigonal lattice.

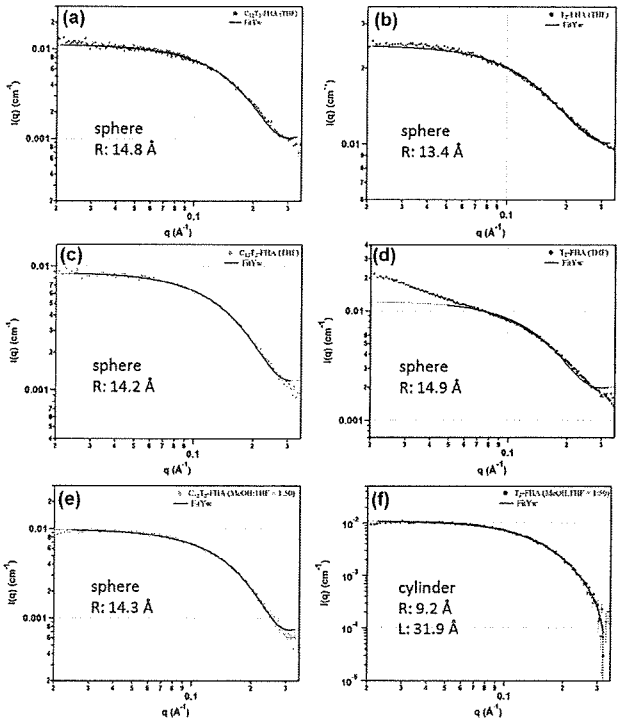

Figure 3. SAXS profiles for the THF solutions of (a) 0.5 mg mL^{-1} $C_{12}T_2$-FHA, (b) 0.5 mg mL^{-1} T_2-FHA, (c) 1 mg mL^{-1} $C_{12}T_2$-FHA, and (d) 1 mg mL^{-1} T_2-FHA, fitted to a sphere form factor model (solid line). SAXS profiles for the solutions of (e) 0.5 mg mL^{-1} $C_{12}T_2$-FHA and (f) 1 mg mL^{-1} T_2-FHA in MeOH:THF (1:50 v/v) fitted to a sphere and a cylinder form factor model (solid line), respectively.

firmed that the HC film has hollow structure and nearly monodispersed pores (pore diameter ≈ 1.6 μm). On the contrary, a birefringent film, which contains pores of different sizes (Figure 2b), was obtained by casting the chloroform ($CHCl_3$) solution of T_2-FHA on a glass substrate. Birefringence of the film indicates that the T_2 arms of the T_2-FHA molecules are self-organized and have an orientational order in the film. The HC patterns have been intensively investigated since the discovery of the self-organized HC morphologies of star-shaped polystyrene by Bernard Francois and coworkers in 1994.[17] The hollow HC array was formed after the evaporation of hexagonally packed, non-coalescing water droplets distributed in polymer solutions prepared by the so-called "breath-figure method".[18] Although the molecular architecture is not the prerequisite for the formation of HC pattern, it does affect the feasibility to obtain the HC patterns. Previous studies showed that highly branched or star-shaped polymers are more feasible to form the well-organized HC array than the linear ones. Thus, although $C_{12}T_2$-FHA and T_2-FHA both are 12-arm star-like molecules, their distinct solid-state morphologies imply that they may adopt different conformations and have different molecular shapes in the thin films.

The final solid-state morphology is a result of sequential molecular assembling during the solvent evaporation process. The FHA molecules may take different conformations because of the changes in the environment and the differences in the peripheral functional groups. To know how the distinct solid-state morphologies of $C_{12}T_2$-FHA and T_2-FHA were developed, we first check the conformational preference of the FHAs in solution by SAXS and ^{1}H NMR (Figure 3, and S9 in the SI). Figure 3 shows the SAXS profiles with the fitted curves and structural parameters obtained from the model fitting for the two FHAs at different conditions. THF was used as the solvent to provide sufficient scattering contrast for the FHA solutions. At a concentration of 0.5 mg mL^{-1} in THF (Figure 3a and 3b), $C_{12}T_2$-FHA and T_2-FHA were fitted to a sphere form factor model with average diameters ($2R_g$) of 2.96 and 2.68 nm, respectively. The $2R_g$ values are smaller than the estimated diameters of the fully extended $C_{12}T_2$-FHA (5.8 nm) and T_2-FHA (3.8 nm) as illustrated in Figure S10, suggesting that the peripheral arms of the FHAs are not fully stretched in the solutions. As shown in Figure 3c and 3e, neither the increase of the solution concentration from 0.5 to 1.0 mg mL^{-1}, nor the presence of 2 v% of methanol (MeOH), which is a poor solvent for the FHAs, significantly change the scattering profile of $C_{12}T_2$-FHA solution. However, the increased solution concentration resulted in the formation of T_2-FHA aggregates, as indicated by the scattering hump at $q = 0.02$–0.05 Å^{-1} in Figure 3d, and the presence of 2 v% of MeOH changes T_2-FHA from spherical shape to a cylinder shape with average diameter of 1.84 nm and length of 3.19 nm (Figure 3f). The SAXS results thus clearly show that both $C_{12}T_2$-FHA and T_2-FHA take a spherical shape in a good solvent, such as THF, but T_2-FHA has a stronger tendency to response to the changes of the solution conditions than $C_{12}T_2$-FHA does. Same tendency was also found in $CHCl_3$ and CS_2, the solvents that were used to prepare the casted films of the two FHAs. As shown in Figure S9, in $CDCl_3$, the signal of H_d on the triazole units of $C_{12}T_2$-FHA and T_2-FHA are observed at $\delta = 7.72$ and 7.73 ppm, and the signal of H_e on the bithiophene units of $C_{12}T_2$-FHA and T_2-FHA are found at $\delta = 7.15$ and 7.18 ppm, respectively. Adding CS_2 into the solutions caused clear downfield shifts of the H_d and H_e signals, indicating the peripheral arms aggregate because of the change of the solvent property. More importantly, while

© 2016 Wiley-VCH Verlag GmbH & Co. KGaA, Weinheim

the H_e signal of **T_2-FHA** completely shifts from $\delta = 7.18$ to 7.22 ppm, the H_e signal of **$C_{12}T_2$-FHA** split into two broad peaks (denoted as H_e and H_{es} in Figure S9) in the CS_2:$CDCl_3$ solution. The complete shift of H_e signal of **T_2-FHA** indicates that the T_2 arms of the FHA have a strong tendency to aggregate. On the contrary, the split H_e signal of the **$C_{12}T_2$-FHA** not only indicate the $C_{12}T_2$ arms have less tendency to aggregate, but also point out the coexistence of the aggregated and non-aggregated domains of the $C_{12}T_2$ arms, implying that **$C_{12}T_2$-FHA** may be in a distorted spherical conformation. Therefore, the ^1H NMR results also support that both FHAs take spherical conformations in a good solvent, such as $CDCl_3$, but their peripheral arms aggregate differently when a poor solvent, such as CS_2, is added into the solutions. Because the terminal dodecyl chains are the only structural difference between **$C_{12}T_2$-FHA** and **T_2-FHA**, different solution behaviors of the two FHAs can be attributed to these flexible chains. Considering the interaction among the 12 peripheral arms of a FHA as intramolecular interactions, such flexible chains thus decrease the intramolecular interaction of the FHA and keep the FHA close to the star conformation.

Finally, the solid-state packing of the FHAs was investigated by selected area electron diffraction (SAED). Figure 2d and S11a show the SAED pattern of the birefringent domain of **T_2-FHA**. The diffraction pattern includes 6 diffraction spots (d-spacing = 0.53 nm) separated by 60° in the azimuthal direction, suggesting **T_2-FHAs** assembled into either a hexagonal or a trigonal lattice. Considering that neither star nor rod conformation has 6-fold rotation symmetry, the hexagonal lattice was excluded. A two-dimensional (2D) primitive trigonal lattice with $a = 1.07$ nm and $\gamma = 120°$, which contains one **T_2-FHA** in a rod conformation per lattice, was built in the software package Accelrys Cerius[2] as shown in Figure 2e. The simulated ED pattern (Figure S12) generated from the trigonal lattice closely matches with the experimental ED pattern. The observed six diffraction spots with d-spacing = 0.53 nm were indexed as (110), ($\bar{1}\bar{1}0$), ($2\bar{1}0$), ($\bar{2}10$), ($\bar{1}20$), and ($1\bar{2}0$) diffractions from the trigonal lattice. The (100), (010), ($\bar{1}00$), ($0\bar{1}0$), ($\bar{1}10$) and ($1\bar{1}0$) diffractions are extinct because of the symmetrical arrangements of the twelve T_2 arms. As shown in Figure 2e, because the lateral length of the trigonal lattice is 1.07 nm, which is only slightly larger than the van der Waals diameter of C_{60} (1 nm), the **T_2-FHA** molecules have to contract their T_2 arms to form the rod conformation so that they can be packed into the trigonal lattice. The trigonal packing maximizes the π–π interactions among the T_2 conjugated arms.

Thus, the π–π interaction among the T_2 arms could be the driving force for the **T_2-FHA** to approach the rod conformation and the trigonal packing. If the FHA films are at the most stable state when the π–π interaction among the peripheral arms is maximized, it is possible that the amorphous HC array of **$C_{12}T_2$-FHA** is metastable because the π–π interaction among the peripheral arms are prevented by the terminal dodecyl chains. To evaluate the relative stability of the HC array, the amorphous HC array of **$C_{12}T_2$-FHA** was annealed under saturated CS_2 vapor (Figure 4). The solvent annealing process turned the ordered HC array first into disordered porous film,

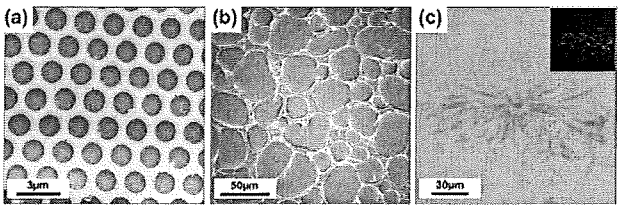

Figure 4. The morphological development of **$C_{12}T_2$-FHA** during the solvent (CS_2) annealing process (a) SEM image of the HC array at $t = 0$, (b) SEM image of the porous film at $t = 10$ mins, and (c) the birefringent dendritic structures at $t = 12$ hrs.

and then eventually to the birefringent dendritic crystals in 12 hrs. The SAED pattern (Figure 2c) of the dendritic crystal confirms that **$C_{12}T_2$-FHA** also change into the rod conformation and pack into a 2D trigonal lattice identical to that of **T_2-FHA**. Slow evaporation of the **$C_{12}T_2$-FHA** solution also facilitated the formation of dendritic crystals (Figure S13). The results prove that the HC phase is a trapped metastable phase, in which **$C_{12}T_2$-FHAs** randomly arrange their vitrified peripheral $C_{12}T_2$ arms. The presence of solvent molecules mobilized the arms and allowed **$C_{12}T_2$-FHAs** to adjust their conformations to pack into the more stable trigonal phase. The SAXS result in Figure S14 further shows a layered structure (d-spacing = 5.77 nm) of **$C_{12}T_2$-FHA** rods along the c-axis. Because only one diffraction peak was observed for the layered structure, **$C_{12}T_2$-FHA** in the adjacent layers does not have long-range positional order. The layered structure was absent in the packing of **T_2-FHA** rods because of the lack of terminal alkyl chains.

To sum up, the conformation and self-organization behaviors of two FHAs, **$C_{12}T_2$-FHA** and **T_2-FHA**, were studied to reveal the conformational preferences and phase stability of FHAs. Although generally considered as spherical particles, our study

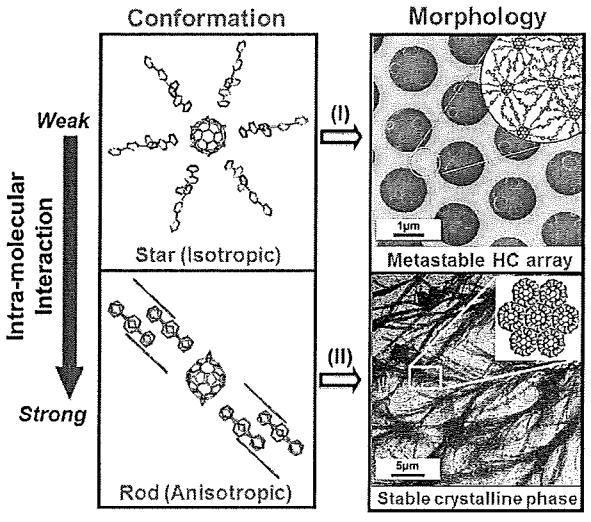

Figure 5. Illustrations of the conformational preferences and self-assembly morphologies of the fullerene hexa-adducts. (I) Vitrification of the FHAs occurs when the solutions of the FHAs were quickly evaporated; (II) crystallization of the FHAs occurs when the solutions of the FHAs were slowly evaporated or when the vitrified films were solvent annealing in a glass chamber.

© 2016 Wiley-VCH Verlag GmbH & Co. KGaA, Weinheim

shows that the FHA can switch its conformation between the star and rod conformation. The conformation preference of a FHA is affected by the strength of the physical interactions among its peripheral arms, that is, the intramolecular interaction of a FHA. As illustrated in Figure 5, poor solvent, such as CS_2 and MeOH, promotes the intramolecular interactions, and drives the FHAs away from the star conformation, whereas the terminal alkyl groups weaken the intramolecular interactions and push the FHAs away from the rod conformation. The *meta*-stable HC array was formed from the FHAs with a more isotropic conformation, but a stable trigonal phase was built with the FHAs in the anisotropic C_3 rod conformation. Because of the large number and high degree of freedom of the peripheral arms, the conformation of FHAs has been a complicated issue for the FHA materials. By using bithiophene as the peripheral unit that has weak physical interactions, our study reveals the conformational preferences and phase stability of the FHAs, and lays a common ground for a discussion of the FHA conformation.

Acknowledgements

This work is supported by the Ministry of Science and Technology, Taiwan (MOST 103-2221-E-009-213-MY3, MOST 104-2628-E-009-007-MY3), and "ATP" of the National Chiao Tung University and Ministry of Education, Taiwan. The authors thank the National Synchrotron Radiation Center for supporting us to carry out the SAXS experiments at beamline BL23A1. The authors also thank Prof. Hsin-Lung Chen at National Tsing Hua University, Taiwan for help with carrying out the SAXS experiments.

Keywords: conformation · conjugated molecule · fullerene · phase stability · self-organization

[1] a) V. Percec, C.-H. Ahn, G. Ungar, D. Yeardley, M. Möller, S. Sheiko, *Nature* **1998**, *391*, 161–164; b) D. E. Discher, A. Eisenberg, *Science* **2002**, *297*, 967–973; c) G. W. Orr, L. J. Barbour, J. L. Atwood, *Science* **1999**, *285*, 1049–1052.

[2] a) H.-J. Sun, S. Zhang, V. Percec, *Chem. Soc. Rev.* **2015**, *44*, 3900–3923; b) N. Seiki, Y. Shoji, T. Kajitani, F. Ishiwari, A. Kosaka, T. Hikima, M. Takata, T. Someya, T. Fukushima, *Science* **2015**, *348*, 1122–1126.

[3] J. Iehl, M. Frasconi, H.-P. Jacquot de Rouville, N. Renaud, S. M. Dyar, N. L. Strutt, R. Carmieli, M. R. Wasielewski, M. A. Ratner, J.-F. Nierengarten, J. F. Stoddart, *Chem. Sci.* **2013**, *4*, 1462–1469.

[4] a) A. Hirsch, O. Vostrowsky, *Eur. J. Org. Chem.* **2001**, 829–848; b) I. Nierengarten, J. F. Nierengarten, *Chem. Rec.* **2015**, *15*, 31–51; c) F. Langa, J.-F. Nierengarten, *Fullerenes: principles and applications*, Royal Society of Chemistry, **2007**.

[5] a) S. Guerra, J. Iehl, M. Holler, M. Peterca, D. A. Wilson, B. E. Partridge, S. Zhang, R. Deschenaux, J.-F. Nierengarten, V. Percec, *Chem. Sci.* **2015**, *6*, 3393–3401; b) M. Helmreich, E. A. Ermilov, M. Meyer, N. Jux, A. Hirsch, B. Röder, *J. Am. Chem. Soc.* **2005**, *127*, 8376–8385; c) T. Chuard, R. Deschenaux, A. Hirsch, H. Schönberger, *Chem. Commun.* **1999**, 2103–2104; d) S. Gottis, C. Kopp, E. Allard, R. Deschenaux, *Helv. Chim. Acta* **2007**, *90*, 957–962; e) F. Beuerle, A. Hirsch, *Chem. Eur. J.* **2009**, *15*, 7447–7455; f) Z. Lin, P. Lu, C. H. Hsu, K. Yue, X. H. Dong, H. Liu, K. Guo, C. Wesdemiotis, W. B. Zhang, X. Yu, *Chem. Eur. J.* **2014**, *20*, 11630–11635; g) S. Campidelli, T. Brandmüller, A. Hirsch, I. M. Saez, J. W. Goodby, R. Deschenaux, *Chem. Commun.* **2006**, 4282–4284; h) P. Yin, Z. Lin, J. Wu, C.-H. Hsu, X. Chen, J. Zhou, P. Lu, S. A. Eghtesadi, X. Yu, S. Z. Cheng, *Macromolecules* **2015**, *48*, 725–731; i) S. Campidelli, C. Eng, I. M. Saez, J. W. Goodby, R. Deschenaux, *Chem. Commun.* **2003**, 1520–1521.

[6] a) K. Yoosaf, J. Iehl, I. Nierengarten, M. Hmadeh, A. M. Albrecht-Gary, J. F. Nierengarten, N. Armaroli, *Chem. Eur. J.* **2014**, *20*, 223–231; b) J. Iehl, J. F. Nierengarten, A. Harriman, T. Bura, R. Ziessel, *J. Am. Chem. Soc.* **2012**, *134*, 988–998.

[7] P. Fortgang, E. Maisonhaute, C. Amatore, B. Delavaux-Nicot, J. Iehl, J. F. Nierengarten, *Angew. Chem. Int. Ed.* **2011**, *50*, 2364–2367; *Angew. Chem.* **2011**, *123*, 2412–2415.

[8] M. Durka, K. Buffet, J. Iehl, M. Holler, J. F. Nierengarten, S. P. Vincent, *Chem. Eur. J.* **2012**, *18*, 641–651.

[9] X. Yu, W. B. Zhang, K. Yue, X. Li, H. Liu, Y. Xin, C.-L. Wang, C. Wesdemiotis, S. Z. D. Cheng, *J. Am. Chem. Soc.* **2012**, *134*, 7780–7787.

[10] a) C.-L. Wang, W.-B. Zhang, H.-J. Sun, R. M. Van Horn, R. R. Kulkarni, C.-C. Tsai, C.-S. Hsu, B. Lotz, X. Gong, S. Z. D. Cheng, *Adv. Energy Mater.* **2012**, *2*, 1375–1382; b) C.-L. Wang, W. B. Zhang, R. M. Van Horn, Y. Tu, X. Gong, S. Z. D. Cheng, Y. Sun, M. Tong, J. Seo, B. B. Hsu, A. J. Heeger, *Adv. Mater.* **2011**, *23*, 2951–2956.

[11] a) C. Bingel, *Chem. Ber.* **1993**, *126*, 1957–1959; b) V. Campisciano, V. La Parola, L. F. Liotta, F. Giacalone, M. Gruttadauria, *Chem. Eur. J.* **2015**, *21*, 3327–3334.

[12] J. Iehl, R. Pereira de Freitas, B. Delavaux-Nicot, J. F. Nierengarten, *Chem. Commun.* **2008**, 2450–2452.

[13] Y. Geng, A. Fechtenkötter, K. Müllen, *J. Mater. Chem.* **2001**, *11*, 1634–1641.

[14] X. Zhao, C. Piliego, B. Kim, D. A. Poulsen, B. Ma, D. A. Unruh, J. M. J. Fréchet, *Chem. Mater.* **2010**, *22*, 2325–2332.

[15] a) J. Iehl, M. Holler, J.-F. Nierengarten, K. Yoosaf, J. M. Malicka, N. Armaroli, B. Delavaux-Nicot, *Aust. J. Chem.* **2011**, *64*, 153–159; b) S. Cecioni, V. Oerthel, J. Iehl, M. Holler, D. Goyard, J. P. Praly, A. Imberty, J. F. Nierengarten, S. Vidal, *Chem. Eur. J.* **2011**, *17*, 3252–3261.

[16] A. Hirsch, I. Lamparth, T. Groesser, H. R. Karfunkel, *J. Am. Chem. Soc.* **1994**, *116*, 9385–9386.

[17] G. Widawski, M. Rawiso, B. Francois, *Nature* **1994**, *369*, 387–389.

[18] a) U. H. F. Bunz, *Adv. Mater.* **2006**, *18*, 973–989; b) W. Wang, C. Du, X. Wang, X. He, J. Lin, L. Li, S. Lin, *Angew. Chem. Int. Ed.* **2014**, *53*, 12116–12119; *Angew. Chem.* **2014**, *126*, 12312–12315; c) P. Escalé, L. Rubatat, L. Billon, M. Save, *Eur. Polym. J.* **2012**, *48*, 1001–1025; d) M. H. Stenzel, C. Barner-Kowollik, T. P. Davis, *J. Polym. Sci. Part A* **2006**, *44*, 2363–2375; e) V.-T. Bui, S. H. Ko, H.-S. Choi, *ACS Appl. Mater. Interfaces* **2015**, *7*, 10541–10547.

Manuscript received: April 19, 2016
Revised: May 9, 2016
Accepted Article published: June 1, 2016
Final Article published: June 22, 2016

© 2016 Wiley-VCH Verlag GmbH & Co. KGaA, Weinheim